M. L. Snapper, A. H. Hoveyda, *J. Am. Chem. Soc.* **1999**, *121*, 4284; e) M. Takamura, Y. Hamashima, H. Usuda, M. Kanai, M. Shibasaki, *Angew. Chem.* **2000**, *112*, 1716; *Angew. Chem. Int. Ed.* **2000**, *39*, 1650; f) E. J. Corey, M. J. Grogan, *Org. Lett.* **1999**, *1*, 157; g) H. Ishitani, S. Komiyama, S. Kobayashi, *Angew. Chem.* **1998**, *110*, 3369; *Angew. Chem. Int. Ed.* **1998**, *37*, 3186; f) H. Ishitani, S. Komiyama, Y. Hasegawa, S. Kobayashi, *J. Am. Chem. Soc*. **2000**, *122*, 762.

[3] Catalytic enantioselective direct Mannich reactions: a) S. Yamasaki, T. Iida, M. Shibasaki, *Tetrahedron* **1999**, *55*, 8857; b) K. Juhl, N. Gathergood, K. A. Jørgensen, *Angew. Chem.* **2001**, *113*, 3083; *Angew. Chem. Int. Ed.* **2001**, *40*, 2995; c) A. Córdova, S.-I. Watanabe, F. Tanaka, W. Notz, C. F. Barbas III, *J. Am. Chem. Soc.* **2002**, *124*, 1842; d) A. Córdova, W. Notz, G. Zhong, J. M. Betancort, C. F. Barbas III, *J. Am. Chem. Soc.* **2002**, *124*, 1866.

[4] K. Juhl, K. A. Jørgensen, *J. Am. Chem. Soc.* **2002**, *124*, 2420.

[5] For an review on asymmetric α-amination reactions see J.-P. Genet, C. Greck, D. Lavergne, *Modern Amination Methods* (Ed.: A. Ricci), Wiley-VCH, Weinheim, **2000**, chap. 3.

[6] D. A. Evans, S. G. Nelson, *J. Am. Chem. Soc.* **1997**, *119*, 6542.

[7] For the use of proline and other chiral amines as catalysts see for example, a) P. I. Dalko, L. Moisan, *Angew. Chem.* **2001**, *113*, 3840; *Angew. Chem. Int. Ed.* **2001**, *40*, 3726; b) A. Córdova, W. Notz, C. F. Barbas III, *J. Org. Chem.* **2002**, *67*, 301; c) K. Sakthivel, W. Notz, T. Bui, C. F. Barbas III, *J. Am. Chem. Soc.* **2001**, *123*, 5260; d) B. List, R. A. Lerner, C. F. Barbas III, *J. Am. Chem. Soc.* **2000**, *122*, 2395; e) J. F. Austin, D. W. C. MacMillan, *J. Am. Chem. Soc.* **2002**, *124*, 1172; f) A. B. Northrup, D. W. C. MacMillan, *J. Am. Chem. Soc.* **2002**, *124*, 2458; g) N. A. Paras, D. W. C. MacMillan, *J. Am. Chem. Soc.* **2001**, *123*, 4370; h) W. S. Jen, J. J. M. Wiener, D. W. C. MacMillan, *J. Am. Chem. Soc.* **2000**, *122*, 9874; i) K. A. Ahrendt, C. J. Borths, D. W. C. MacMillan, *J. Am. Chem. Soc.* **2000**, *122*, 4243; j) A. Bøgevig, N. Kumaragurubaran, K. A. Jørgensen, *Chem. Commun*. **2002**, 620.

[8] The enantiomeric excess was 77% and full conversion was obtained after only 2 min reaction time!

[9] Absolute configuration of **5**: W. A. Kleschick, M. W. Reed, J. Bordner, *J. Org. Chem.* **1987**, *52*, 3168.

[10] S. J. Katz, S. C. Bergmeier, *Tetrahedron Lett.* **2002**, *43*, 557.

[11] Absolute configuration of **6**: M. J. Burk, J. G. Allen, *J. Org. Chem.* **1997**, *62*, 7054.

A New Trend in Phenalenyl Chemistry: A Persistent Neutral Radical, 2,5,8-Tri-*tert*-butyl-1,3-diazaphenalenyl, and the Excited Triplet State of the Gable *syn*-Dimer in the Crystal of Column Motif**

Yasushi Morita,* Takashi Aoki, Kozo Fukui, Shigeaki Nakazawa, Koichi Tamaki, Shuichi Suzuki, Akira Fuyuhiro, Kagetoshi Yamamoto, Kazunobu Sato, Daisuke Shiomi, Akira Naito, Takeji Takui,* and Kazuhiro Nakasuji*

Phenalenyl (**1**) is a highly symmetric (D_{3h}) odd alternating-hydrocarbon π radical, found as early as 1956,[1] and it still plays an important role as a building block for spin-mediated molecular functions in organic molecule-based magnets,[2] and organic metal and conducting materials.[3] Recent progress in phenalenyl chemistry has been made in the isolation of the radical itself in the crystalline state by employing bulky substituents (**2**[4a] and perchlorophenalenyl[4b]), with the exploration of amphoteric redox systems[5] which have intriguing potential applications, such as organic molecular batteries,[6] and with the synthesis of novel phenalenyls with extended conjugation, such as compound **3**.[7] 1,3-Diazaphenalenyl (**4**) is a typical example of the isoelectronic mode of heteroatomic modification for phenalenyl. Successful isolation of **2**[4] aided by the steric hindrance induced by the bulky

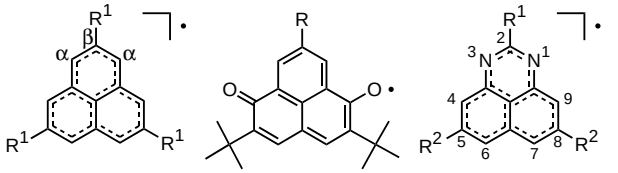

1 R^1 = H
2 R^1 = *t*Bu

3

4 $R^1 = R^2$ = H
5 R^1 = *t*Bu, R^2 = H
6 $R^1 = R^2$ = *t*Bu

[*] Prof. Dr. Y. Morita, Prof. Dr. K. Nakasuji, T. Aoki, Dr. K. Tamaki, S. Suzuki, Prof. Dr. A. Fuyuhiro, Prof. Dr. K. Yamamoto
Department of Chemistry, Graduate School of Science
Osaka University
Toyonaka, Osaka 560-0043 (Japan)
Fax: (+81) 6-6850-5395
E-mail: nakasuji@chem.sci.osaka-u.ac.jp

Prof. Dr. T. Takui, Dr. K. Fukui, Dr. S. Nakazawa, Prof. Dr. K. Sato, Prof. Dr. D. Shiomi
Departments of Chemistry and Materials Science
Graduate School of Science
Osaka City University
Sumiyoshi-ku, Osaka 558-8585 (Japan)
Fax: (+81) 6-6605-3137
E-mail: takui@sci.osaka-cu.ac.jp

Prof. Dr. A. Naito
Faculty of Engineering, Yokohama National University
Hodogaya-ku, Yokohama 240-0085 (Japan)

[**] This work has been supported by Grants-in-Aid for General Scientific Research and Scientific Research on Priority Area "Delocalized π-Electronic Systems (No. 297)" from the Ministry of Education, Culture, Sports, Science, and Technology, Japan.

Supporting information for this article is available on the WWW under http://www.angewandte.com or from the author.

  1433-7851/02/4110-1793 $ 20.00+.50/0

groups at the β-positions (2-, 5-, and 8-positions) has encouraged us to synthesize 2,5,8-tri-*tert*-butyl-1,3-diazaphenalenyl (**6**), which has led to the isolation of such a radical as crystalline solid for the first time, in contrast to a pioneering attempt by Sabanov et al. for compound **5**.[8] The synthesis, electronic structure, and a gable *syn*-dimerization of **6** in the crystal structure, which has a column motif, are reported here. Interestingly, the column structure motif is a counterpart of the herringbone one of homoatomic phenalenyl **2**.

The precursor, 2,5,8-tri-*tert*-butyl-1,3-diazaphenalene (**7**; Scheme 1), was prepared from *tert*-butylated dinitronaphthalene **8**[9] in two steps: 1) reduction with Sn, $SnCl_2 \cdot 2H_2O$ under acidic conditions, 2) condensation with *t*BuCHO followed by the dehydrogenation with Pd/C catalyst.[10] Treatment of **7** with active PbO_2 and recrystallization gave **6** as green crystals (Scheme 1).[11] The radical **6** in the crystal is stable in the absence of air. In air the radical decomposes slowly, but most of it remains unchanged for weeks, thus showing higher stability than **2**.[4a] The increased stability resulting from the heteroatomic modification in the π conjugation is contrary to the claim by Sabanov et al. for **5**.[8]

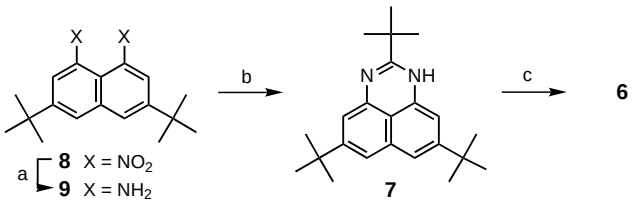

Scheme 1. Synthetic route for **6**. Reagents and conditions: a) Sn (4.3 equiv), $SnCl_2 \cdot 2H_2O$ (7.9 equiv), conc. HCl:AcOH (1:1), 100 °C, 5 h, 82 %; b) *t*BuCHO (1.3 equiv), 3 mol % Pd/C, xylene, reflux, 3.5 h, 77 %; c) PbO_2 (5 equiv), degassed benzene, RT, 1.5 h, recrystallized from hexane, 42 %.

To clarify the bulk magnetic properties of the crystalline state of **6**, the magnetic susceptibility χ_p of a polycrystalline sample was measured from 1.8 to 350 K at 0.1 T.[12] Below 250 K **6** exhibits a weak paramagnetism from impurity radicals (ca. 0.1 %) presumably arising from lattice defects. The result shows that molecular assemblies of **6** in the crystal are in the spin-singlet state, thus revealing the dimerization of **6**. Dissolution of this solid sample in organic solvents gave the strong ESR signals characteristic of **6**, confirming that **6** remains stable and unchanged in the crystal under inert atmosphere. On raising the temperature to 350 K, a small but significant increase in $\chi_p T$ was observed, which suggests the possible existence of thermally accessible paramagnetic states.

To identify such a thermally activated paramagnetic state, cw-ESR (cw = continuous wave) spectra were measured for the solid sample of **6** (Figure 1 a). In addition to the central intense signal from the monoradical impurities, fine-structure triplet-state ESR signals ($\Delta M_S = \pm 1$ allowed transitions) with axial symmetry are clearly seen. The spectral simulation yielded spin-Hamiltonian parameters $S = 1$, $g = 2.004$, $|D|/hc = 0.0173\ cm^{-1}$, and $|E|/hc < 10^{-3}\ cm^{-1}$. The temperature dependence of the triplet signal intensity was best described by a singlet–triplet model[13] with an energy gap of $2J/k_B = -4.19(2) \times 10^3$ K (Figure 1 b). The results seemingly resemble

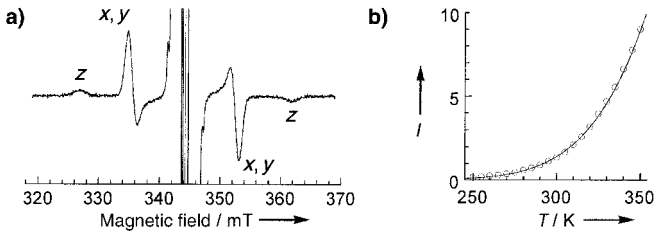

Figure 1. a) Observed triplet-state ESR spectrum of the powder sample of **6** at 350 K. The *x*, *y*, and *z* denote the canonical absorption peaks. The microwave frequency used is 9.638615 GHz. b) Temperature dependence of the triplet signal intensity ○ = observed, —— = calculated; $2J/k_B = -4.19 \times 10^3$ K.

those for **2** ($S = 1$, $g = 2.003$, $|D|/hc = 0.0167\ cm^{-1}$, $|E|/hc < 10^{-3}\ cm^{-1}$, and $2J/k_B = -3.34(3) \times 10^3$ K), but the values for **6** are larger than those for **2**. The comparison suggests that **6** also forms a dimer structure with a face-to-face staggered arrangement. Such an arrangement ensures minimum steric repulsion between the *tert*-butyl groups, but the bonding character of the dimerization of **6** is different from that in **2**.

The X-ray crystal-structure analysis[14] gives a rationale for the difference in the D and $2J/k_B$ values between **2** and **6**. Figure 2 a and b show ORTEP views of the *syn*-dimer of **6** with a gable structure. In the gable *syn*-dimer the shortest distance between the α-carbon sites is 0.215 nm and the longest one

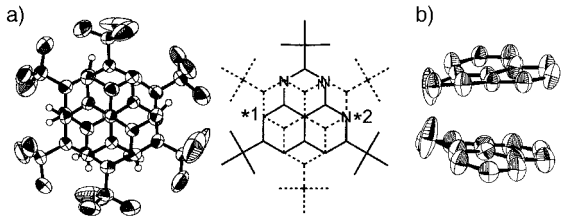

Figure 2. ORTEP views of the gable *syn*-dimer of **6**. a) Top view and a schematic representation; the nitrogen sites are located in terms of the most probable face-to-face arrangement; *1: the shortest C–C distance and *2: the longest distance between the α-carbon and nitrogen sites (see text). b) Side view; the *tert*-butyl groups are omitted for clarity.

between the α-carbon and the nitrogen sites is 0.379 nm, in contrast to the pancake-type stacking of symmetric pure π-dimerization for **2** (0.320–0.332 nm).[4a] The gable *syn*-dimer structure for **6** and asymmetric bonding nature formed in the dimer are induced by the symmetry-breaking incorporation of nitrogen atoms at the 1- and 3-positions. The dimer packing mode is a column structure for **6** (see Supporting Information), which is important in organic metals and conducting materials,[3a,b] whereas the herringbone structure for **2** does not give properties that are relevant for these areas.[4a]

The observed very low E value ($|E|/hc < 10^{-3}\ cm^{-1}$) for **6** reflects axially symmetric nature of the dipolar spin–spin interaction in the excited triplet state of the dimer. The assumed dimer structure, however, does not straightforwardly lead to the electronic structure with a threefold or greater axial symmetry because of the symmetry lowering caused by the incorporated nitrogen atoms. Indeed, ^{13}C cross-polarization magic-angle spinning (CPMAS) solid-state NMR measurements of the molecular crystal at room temperature

  1433-7851/02/4110-1794 $ 20.00+.50/0 *Angew. Chem. Int. Ed.* **2002**, *41*, No. 10

indicated the lower symmetric (C_1) dimerization of **6** in the singlet ground state. A rationale for the low E value is that the dipolar spin–spin interaction within the *syn*-dimer molecule undergoes averaging and smearing out of a small amount of the departure from the axial symmetry as a result of inhomogeneous hyperfine broadening in the fine-structure spectra, which gives rise to an apparent high symmetry with a more than threefold rotation axis.

To evaluate the heteroatomic effects of **6** induced by a pair of nitrogen atoms, the π-spin-density distribution of **6** was determined by liquid-phase ESR and ENDOR/TRIPLE spectroscopy. Under inert atmosphere, **6** in a toluene solution was extremely stable in contrast to **5**.[8] The ESR spectrum is interpreted by ^{1}H-, ^{14}N-, and ^{13}C (1.1 %) hyperfine couplings as summarized in Table 1. The π-spin densities on the nitrogen and carbon sites were determined by the observed couplings with the help of McConnell and Heller–McConnell equations, respectively. To determine the π-spin densities on the other carbon sites without protons, the Fraenkel–Karplus equation was applied. Such an empirical treatment gave all the π-spin densities, as depicted in Figure 3. It appears that a robust π-spin polarization similar to the parent phenalenyl radical **1** is maintained in **6** in spite of the heteroatomic modification, which gives rise to the alternation of the signs of the π spin densities between the neighboring sites. By comparing the spin densities of **6** with those of **2**,[4a] it appears that the spin densities of the 1- and 3-positions decrease appreciably, while those of the 4-, 6-, 7-, and 9-positions increase, that is, these four sites become more "active" following the heteroatomic perturbation. Nevertheless, the presence of the bulky substituents at the 5- and 8-positions contributes to the chemical stabilization of the 1,3-diazaphenalenyl π system.

Table 1. Hyperfine coupling constants (hfccs) of ^{1}H, ^{13}C, and ^{14}N nuclei, and g value.[a]

a^H [mT]				a^N [mT]		g Value
4, 9	6, 7	2-*t*Bu	5, 8-*t*Bu	1, 3		2.0033
−0.638	−0.715	+0.006	+0.021	+0.292		
			a^C [mT]			
2	4, 9	5, 8	6, 7	10, 11	12	13
−0.550	+0.880	−0.820	+1.087	−0.654	−0.885	+0.081

[a] Assignments of hfccs were based on DFT calculation by using Gaussian 94 with SVWN/6–31G*//SVWN/6-31G* method.

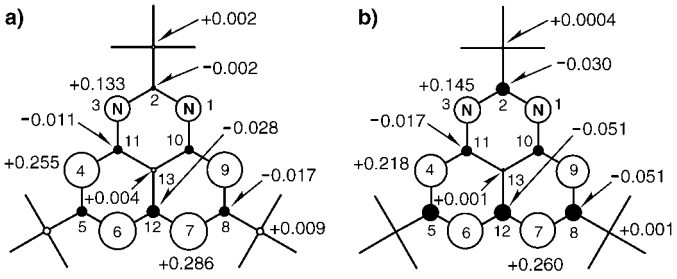

Figure 3. π-spin-density distribution of **6** a) experimentally determined and b) calculated by DFT method using Gaussian 94 (SVWN/6–31G*//SVWN/6-31G*). Open and filled circles denote positive and negative spin densities, respectively.

The spin structure of **6** is in harmony with such a gabled face-to-face arrangement of the *syn*-dimer in the crystal. In such an arrangement maximum orbital overlaps occur between the α-carbon sites with largest and next-largest spin densities, which causes a strong bonding interaction ($2J/k_B = -4.19(2) \times 10^3$ K) between the radicals in the *syn*-dimer of **6**. The reflection spectroscopy and the refined X-ray crystal-structural analysis of **6** and other azaphenalenyls are underway. To our knowledge, the *syn*-dimer of **6** is not only the first example that exhibits a column crystal-structure motif with pseudo π dimerization between neutral organic radicals,[15] but also diverse potentials, such as those of organic conducting materials. In contrast to the herringbone motif for the pure π-dimer **2**, the finding of the gable *syn*-dimer with the column motif for **6** derived by the heteroatomic modification should be of interest in crystal engineering and organic materials science.

Received: February 25, 2002 [Z18760]

[1] a) D. H. Reid, *Chem. Ind. (London)* **1956**, 1504–1505; b) P. B. Sogo, M. Nakazaki, M. Calvin, *J. Chem. Phys.* **1957**, *26*, 1343–1345.

[2] For a recent overview, see: a) *Molecular Magnetism* (Eds.: K. Itoh, M. Kinoshita), Kodansha, and Gordon and Breach Science Publishers, **2000**, pp. 1–347; b) *Magnetic Properties of Organic Materials* (Ed.: P. M. Lahti), Marcel Dekker, New York, **1999**, pp. 1–728.

[3] a) R. C. Haddon, *Nature* **1975**, *256*, 394–396; b) R. C. Haddon, *Aust. J. Chem.* **1975**, *28*, 2343–2351; c) X. Chi, M. E. Itkis, B. O. Patrick, T. M. Barclay, R. W. Reed, R. T. Oakley, A. W. Cordes, R. C. Haddon, *J. Am. Chem. Soc.* **1999**, *121*, 10395–10402; d) K. Tamaki, Y. Morita, J. Toyoda, H. Yamochi, G. Saito, K. Nakasuji, *Tetrahedron Lett.* **1997**, *38*, 4583–4586.

[4] a) K. Goto, T. Kubo, K. Yamamoto, K. Nakasuji, K. Sato, D. Shiomi, T. Takui, M. Kubota, T. Kobayashi, K. Yakushi, J. Ouyang, *J. Am. Chem. Soc.* **1999**, *121*, 1619–1620; b) P. A. Koutentis, Y. Chen, Y. Cao, T. P. Best, M. E. Itkis, L. Beer, R. T. Oakley, A. W. Cordes, C. P. Brock, R. C. Haddon, *J. Am Chem. Soc.* **2001**, *123*, 3864–3871.

[5] T. Kubo, K. Yamamoto, K. Nakasuji, T. Takui, I. Murata, *Bull. Chem. Soc. Jpn.* **2001**, *74*, 1999–2009.

[6] Y. Morita, S. Nishida, J. Kawai, K. Fukui, S. Nakazawa, K. Sato, D. Shiomi, T. Takui, K. Nakasuji, *Org. Lett. in press.*

[7] Y. Morita, T. Ohba, N. Haneda, S. Maki, J. Kawai, K. Hatanaka, K. Sato, D. Shiomi, T. Takui, K. Nakasuji, *J. Am. Chem. Soc.* **2000**, *122*, 4825–4826.

[8] V. Kh. Sabanov, E. S. Klimov, I. V. Bogdanova, E. P. Trub, N. T. Berberova, O. Yu. Okhlobistin, *Khim. Geterotsikl. Soedin.* **1986**, 970–972. They reported that **5** was unstable because of an increase in spin density at the nitrogen sites.

[9] K.-H. Koch, K. Müllen, *Chem. Ber.* **1991**, *124*, 2091–2100.

[10] Selected physical data: **7**, m.p. 267–268 °C; ^{1}H NMR ($CDCl_3$/CF_3COOH; 270 mHz): $\delta = 1.29$ (s, 18), 1.49 (s, 9), 6.93 (d, $J =$ 1.2 Hz), 7.27 ppm (d, $J = 1.2$ Hz); IR (KBr): $\tilde{\nu} = 3320$ cm^{-1}; EI-MS, m/z 336 (M^+, 100 %); elemental analysis calcd (%) for $C_{23}H_{32}N_2$: C 82.09, H 9.59, N 8.33; found: C 82.30, H 9.65, N 8.17.

[11] Selected physical data: **6**, m.p. 164–166 °C; TLC $R_f = 0.62$ (5:1 hexane:ethyl acetate); TLC (alumina) $R_f = 0.58$ (10:1 hexane:ethyl acetate); elemental analysis calcd (%) for $C_{23}H_{31}N_2$: C 82.33, H 9.31, N 8.35, found: C 82.04, H 9.42, N 8.23.

[12] The diamagnetic susceptibility χ_{dia}: -219.7×10^{-6} emu mol^{-1}.

[13] B. Bleaney, K. D. Bowers, *Proc. R. Soc. London Ser. A* **1952**, *214*, 451–465.

[14] The X-ray structure analysis was performed for **6** with an isotopic enrichment of ^{15}N at room temperature: $C_{46}H_{62}{}^{15}N_4$, $M_r = 675.00$, crystal dimensions $0.20 \times 0.10 \times 0.08$ mm^3, pale green, Rigaku/MSC

Mercury CCD diffractometer, $Mo_{K\alpha}$ radiation, $T = 23.0\,^{\circ}C$, monoclinic, space group $P2_1/n$ (No. 14), $a = 12.783(1)$, $b = 21.697(2)$, $c = 15.441(2)$ Å, $\beta = 105.957(4)^{\circ}$, $V = 4117.7(7)$ Å^3, $Z = 4$, $\rho_{calcd} = 1.082\,g\,cm^{-3}$, 28321 reflections collected, 4934 unique intensities reflections observed $[I > 4.00\sigma(I)]$, $2\theta_{max} = 55.0^{\circ}$, structure solution with direct methods (SIR92) and refinement on F with 483 parameters, R (R_w) = 0.153 (0.396), S (GOF) = 2.23. CCDC-183912 (**6**) contains the supplementary crystallographic data for this paper. These data can be obtained free of charge via www.ccdc.cam.ac.uk/conts/retrieving.html (or from the Cambridge Crystallographic Data Centre, 12, Union Road, Cambridge CB2 1EZ, UK; fax: (+44) 1223-336-033; or deposit@ccdc.cam.ac.uk).

[15] For pure π dimerization, see: a) M. R. Gleiter, B. Kanellakopulos, C. Krieger, F. A. Neugebauer, *Liebigs Ann.* **1997**, 473–483, and references therein; b) P. A. Capiomont, B. Chion, J. Lajzérowicz, *Acta Crystallogr. Sect. B* **1971**, *27*, 322–326.

Expanding the Reaction Scope of DNA-Templated Synthesis**

Zev J. Gartner, Matthew W. Kanan, and David R. Liu*

The translation of amplifiable information into chemical structure is a key component of nature's approach to generating functional molecules. The ribosome accomplishes this feat by catalyzing the translation of RNA sequences into proteins. Developing general methods to translate amplifiable information carriers into synthetic molecules may enable chemists to evolve non-natural molecules in a manner analogous to the cycles of translation, selection, amplification, and diversification currently used by nature to evolve proteins. As an initial step towards this goal, we recently examined the generality of DNA-templated synthetic chemistry.[1, 2] We demonstrated the ability of DNA-templated synthesis to direct a modest collection of chemical reactions without requiring the precise alignment of reactive groups into DNA-like conformations. Indeed, the distance independence and sequence fidelity of DNA-templated synthesis allowed the simultaneous, one-pot translation of a model library of more than 1000 templates into the corresponding thioether products, one of which was enriched by in vitro selection for binding to the protein streptavidin and amplified by the polymerase chain reaction (PCR).

The range of reactions known to be supported by DNA-templated synthesis,[2] however, remains a tiny fraction of those used either by synthetic chemists or by nature to generate molecules with desired properties. Many reactions central to the construction of natural or synthetic molecules have yet to be developed in a DNA-templated format despite their known compatibility with water.[3] We describe here the development of several useful DNA-templated reactions, including the first reported DNA-templated organometallic couplings and carbon–carbon bond forming reactions other than pyrimidine photodimerization.[4, 5] Collectively, these reactions represent an important additional step towards the in vitro evolution of non-natural synthetic molecules by enabling the DNA-templated construction of a much more diverse set of structures than has been previously achieved.

We first investigated the ability of DNA-templated synthesis to direct reactions that require a non-DNA-linked activator, catalyst, or other reagent in addition to the principal reactants. To test the ability of DNA-templated synthesis to mediate such reactions without requiring structural mimicry of the DNA backbone, we performed DNA-templated reductive aminations between amine-linked template **1** and benzaldehyde- or glyoxal-linked reagents (**2** and **3**) with millimolar concentrations of $NaBH_3CN$ at room temperature in aqueous solutions. Products formed efficiently when the template and reagent sequences were complementary. In contrast, control reactions in which the sequence of the reagent did not complement that of the template, or in which $NaBH_3CN$ was omitted, yielded no significant product (Table 1 and Figure 1). While DNA-templated reductive aminations to generate products closely mimicking the structure of double-stranded DNA have been previously reported,[6, 7] the above results demonstrate that reductive amination to generate structures unrelated to the phosphoribose backbone can take place efficiently and sequence specifically. We also performed DNA-templated amide bond formations[8, 9] between amine-linked templates **4** and **5** and carboxylate-linked reagents **6**–**9** mediated by 1-(3-dimethylaminopropyl)-3-ethylcarbodiimide (EDC) and *N*-hydroxysulfosuccinimide (sulfo-NHS) to generate amide products in good yields at pH 6.0 and 25 °C (Table 2). Product formation was sequence specific, dependent on the presence of EDC, and surprisingly insensitive to the steric encumbrance of the amine or carboxylate group. Efficient DNA-templated amide formation was also mediated by the water-stable activator 4-(4,6-dimethoxy-1,3,5-triazin-2-yl)-4-methylmorpholinium

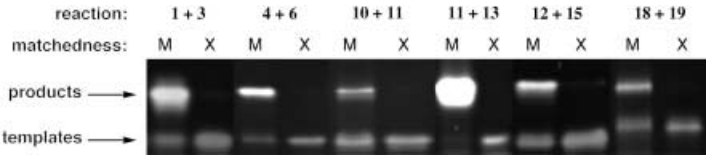

Figure 1. Analysis by denaturing polyacrylamide gel electrophoresis of representative DNA-templated reactions listed in Tables 1 and 2. The structures of reagents and templates correspond to the numbering in Tables 1 and 2. Lanes 1, 3, 5, 7, 9, and 11: reaction of matched (complementary) reagents and templates under the conditions listed in Tables 1 and 2 (the reaction of **4** and **6** was mediated by DMT-MM). Lanes 2, 4, 6, 8, 10, and 12: reaction of mismatched (noncomplementary) reagents and templates under conditions identical to those used in lanes 1, 3, 5, 7, 9, and 11, respectively.

[*] Prof. D. R. Liu, Z. J. Gartner, M. W. Kanan
Department of Chemistry and Chemical Biology
Havard University
12 Oxford Street, Cambridge, MA 02138 (USA)
Fax: (+1) 617-496-5688
E-mail: drliu@fas.harvard.edu

[**] Funding was generously provided by the Searle Scholars Program (00-C-101), an Office of Naval Research Young Investigator Award (N0014-00-1-0596), a Research Corporation Research Innovation Award, and Harvard University. Z.J.G. and M.W.K are supported by NSF Graduate Research Fellowships.

  1433-7851/02/4110-1796 $ 20.00+.50/0